Journal of Physics and Chemistry of Solids 73 (2012) 1282–1289

Contents lists available at SciVerse ScienceDirect

Journal of Physics and Chemistry of Solids

journal homepage: www.elsevier.com/locate/jpcs

Buckling analysis of carbon nanotube bundles under axial compressive, bending and torsional loadings via a structural mechanics model

Ali Lashkari Zadeh [a], Mahmoud Shariati [a,*], Hamid Torabi [b]

[a] Department of Mechanical Engineering, Shahrood University of Technology, Daneshgah Blvd, Shahrood, Iran
[b] Young Researchers Club, Mashhad Branch, Islamic Azad University, Mashhad, Iran

ARTICLE INFO

Article history:
Received 24 July 2011
Received in revised form
10 May 2012
Accepted 19 June 2012
Available online 26 June 2012

Keywords:
A. Nanostructures
D. Mechanical properties

ABSTRACT

A structural mechanics model is employed for the investigation of the buckling behavior of carbon nanotube bundles of three single-walled carbon nanotubes (SWCNTs) under axial compressive, bending and torsional loadings. The effects of van der Waals (vdW) forces are further modeled using a nonlinear spring element.

The effects of different types of boundary conditions are studied for nanotubes with various aspect ratios. The results reveal that bundles comprising longer SWCNTs exhibit lower critical buckling load. Moreover, for the fixed-free boundary condition the rate of critical buckling load reduction is highest, while the lowest critical buckling load occurs. Simulations show good agreement between our model and molecular dynamics results.

1. Introduction

In 1991, the amazing structure of carbon atoms called a carbon nanotube was discovered by Ijima [1]. Nanotubes have received much attention recently due to their high structural stability and fascinating mechanical properties. However, a well-known behavior of CNTs is intertube bonding due to weak van der Waals (vdW) interactions, which results in formation of bundles that contain hundreds or thousands of individual nanotubes. In general, existing researches in this area are very limited.

Yakobson et al. [2] conducted systematic molecular dynamics (MD) simulations on basic mechanical behavior of SWCNTs. After comparing their results with those predicted by thin shell theory, they suggested that buckling behavior of a SWCNT can be well predicted by a shell model and thereby fitted both a value for Young's modulus (~5.5 TPa) and for the effective thickness of the CNTs (t=0.066 nm). Lu [3] has investigated elastic properties of nanotubes and SWCNT bundles by using an empirical force constant model. Young's modulus of ~1 TPa and shear modulus of ~0.5 TPa were reported based on a simulated tensile test. Furthermore, an atomic force microscope and a special substrate has been used by Salvetat et al. [4] and the elastic and shear moduli of individual SWNT ropes were measured to be of the order of 1 TPa and 1 GPa, respectively. Chang [5] studied the torsional behavior of a chiral SWCNT and found it to be dependent on the loading directions due to the structural symmetry of the SWCNT.

Yang et al. [6] performed atomistic simulations to investigate the torsional behavior of abnormal double-walled carbon nanotubes (DWCNTs) with an interlayer distance of less than 0.34 nm and carbon nanowires (CNWs) made of linear carbon-atom chain (C-chain) encapsulated inside single-walled carbon nanotubes (SWCNTs) subject to torsional motion. They modeled interaction between atoms using the second-generation reactive empirical bond-order potential coupled with the Lennard–Jones potential. Yang and Wei [7] presented another study in which the torsional behavior of DWCNTs with and without some interwall sp3 bonds subject to torsion motion has been investigated.

Ru [8] made use of a modified honeycomb model to study the elastic buckling of CNT bundles under high pressure. Qian et al. [9] used molecular mechanics and molecular dynamics to study the nature of load transfer in a SWCNT bundle consisting of seven (10, 10) SWCNTs. Liew et al. [10] studied the tensile and compressive properties of CNT bundles by using the molecular dynamics simulations, with the atomic interactions modeled by the short-range Brenner potential coupled with the long-range vdW potential. Yakobson and Couchman [11] presented a connection between the stiffness of CNTs and their mesoscopic physical behavior. Persistence lengths of CNT and bundles were calculated and shown to be in macroscopic range (0.03–1 mm for an individual tube), exceeding by many orders of magnitude the typical diameters (around 1–3 nm). Cranford [12] represented individual CNTs by a simple single degree of freedom (SDOF)

* Corresponding author. Tel.: +98 915 1014452; fax: +98 511 6026593.
E-mail address: mshariati44@gmail.com (M. Shariati).

0022-3697/$ - see front matter © 2012 Elsevier Ltd. All rights reserved.
http://dx.doi.org/10.1016/j.jpcs.2012.06.014

"lollipop" model to investigate the formation, mechanics, and self-organization of CNT bundles driven by weak vdW interactions.

Due to the application of carbon nanotubes in various industries, mechanical analysis of these nanotubes under different loading and boundary conditions is necessary. Amongst these analyses, buckling is very important. Thus, we have tried to predict the critical buckling loads, moments and torques of CNTs bundle under axial compressive, bending and torsional loadings via a structural mechanics approach. Moreover, the effects of intertube vdW interactions on these nanotubes are investigated.

2. Structural model

Carbon nanotubes have superior mechanical properties, for this reason many structures are developed each day. In a SWCNT, the total steric potential energy is the sum of energies due to interactions between carbon atoms. The detailed derivation procedure for the formulation and other features of this model can be found in our previous work [13]:

$$u_{total} = u_r + u_\theta + u_\varphi + u_\omega + u_{vdw} \tag{1}$$

where u_r, u_θ, u_ϕ, u_ω and u_{vdw} are bond energies associated with bond stretching, angle variation or bond bending, dihedral angle torsion, out-of-plane torsion and vdW forces (noncovalent), respectively.

$$u_r = D_e\left\{\left[1-e^{-\beta(r-r_0)}\right]^2-1\right\} \tag{2}$$

$$u_\theta = 1/2K_\theta(\theta-\theta_0)^2\left[1+K_{sextic}(\theta-\theta_0)^4\right] \tag{3}$$

$$u_\phi = 1/2K_\phi\left[1+\cos\left(n\phi-\phi_0\right)\right]o \tag{4}$$

$$u_\omega = 1/2k_\omega[1+\cos(n\omega\text{-}w_0)]o \tag{5}$$

In this paper, Morse potentials are used for stretching and bending potentials, and for torsion and out-of-plane torsion interactions a periodic type of bond torsion is employed. The parameters at these potentials are listed in Table 1 [14]. The stretch force, the angle variation moment, the dihedral angle torque, and out-of-plane torque can be obtained from differentiations of Morse potentials as functions of bond stretch, bond angle, dihedral angle, and out-of-plane angle variation, respectively.

Table 1
Parameters for molecular mechanics potentials.

Interaction	Parameters
u_r	D_e=0.6031 nN nm, β=26.25 nm^{-1}, r_0=0.142 nm
u_θ	$K_\theta = 1.42$ nN nm/Rad^{-2}, $K_{sextic} = 0.754$ nm^{-4}, $\theta_0 = 120^\circ$
u_φ	$K_\phi = 0.278$ nN nm/Rad^{-2}, $n=2$, $\phi_0 = 180^\circ$
u_w	$K_\omega = 0.278$ nN nm/Rad^{-2}, $n=2$, $\omega_0 = 180^\circ$

In the present structural model, carbon atoms are simulated in ABAQUS software with discrete rigid spheres and the interactions between them are modeled with spring and connector elements which are adjoined to reference points at the center of each sphere. A nonlinear connector is considered for modeling of the stretching and torsional interactions and a nonlinear spring for modeling of the angle variation interaction (see Fig. 1). Every carbon atom in ABAQUS/CAE has a reference point and a local coordinate at the center of the sphere. The local coordinate consists of a Cartesian coordinate for stretching and a rotational coordinate for torsion. The directions of all local coordinates have one rule, the X direction of these coordinates is in the connector direction, and the Z direction is vertical to the central axis of the nanotube. Because we can only use a linear spring in the CAE space of ABAQUS, by changing the linear spring command to a nonlinear spring command in the input file, and by applying the nonlinear data for $F(\Delta R)$ versus ΔR using Eq. (7), we can apply the bond bending spring to the model. For applying bond stretch and torsion forces to the connectors, we can apply the nonlinear stiffnesses in three directions (X, Y, and Z) directly. For stretching stiffness in the X direction, we can obtain the nonlinear data for $F(\Delta r)$ versus Δr by Eq. (6), and for torsional stiffness in X direction, we can obtain the nonlinear data for $T(\Delta\varphi)$ versus $\Delta\phi$ by Eq. (8). For torsional stiffness in the Y direction, we can obtain the nonlinear data for $T(\Delta\omega)$ versus $\Delta\omega$ by Eq. (9).

$$F(r-r_0) = 2\beta D_e\left[1-e^{-\beta(r-r_0)}\right]e^{-\beta(r-r_0)} \tag{6}$$

$$F(R-R_0) = \frac{4}{r_0^2}k_\theta(R-R_0)\left[1+\frac{16}{r_0^4}\left(1+\frac{4}{r_0^2}\right)k_{\text{sextic}}(R-R_0)^4\right] \tag{7}$$

$$T(\varphi-\varphi_0) = 1/2k_\varphi n\sin\left(n\varphi-\varphi_0\right) \tag{8}$$

$$T(\omega-\omega_0) = 1/2k_\omega n\sin(n\omega-\omega_0) \tag{9}$$

This structural model was successfully used for predicting the Young's modulus [15], natural frequencies [16] and axial buckling behavior of perfect and defective SWCNTs [13,17]. In the following, the molecular structural mechanics method is extended to treat the buckling behavior of CNT bundles by taking into account the vdW forces acting between the neighboring tube layers. The noncovalent interactions like vdW forces can be adequately described using Lennard–Jones potential [18,19]. The corresponding energy is given by

$$V(r) = 4\varepsilon\left[\left(\frac{\sigma}{r}\right)^{12}-\left(\frac{\sigma}{r}\right)^{6}\right] \tag{10}$$

In Eq. (10) the terms r (in nm) and ε (in kJ/mol) are defined as the Lennard–Jones parameters. They are material specific and determine the nature and strength of the interaction. The term

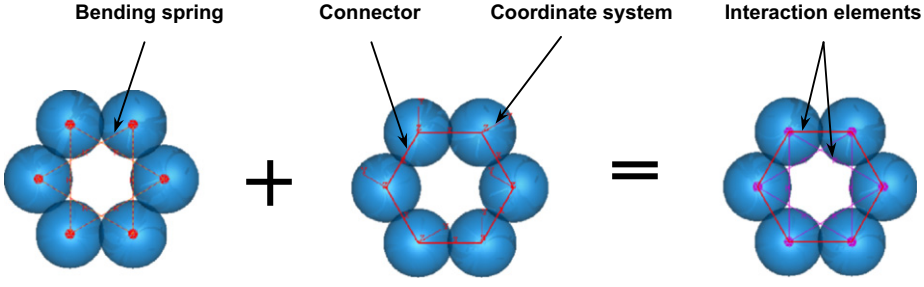

Fig. 1. Spring and connector elements corresponding to the interaction of atoms. (a) The angle variation interaction, (b) the stretching and torsional interactions, and (c) total interaction.

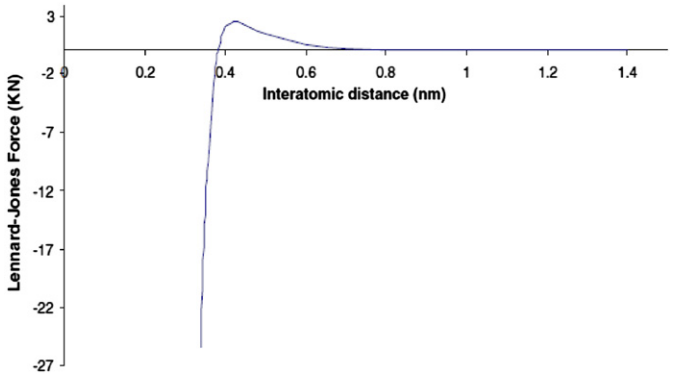

Fig. 2. Variation of the Lennard–Jones force with inter-atomic distance of carbon atoms [9].

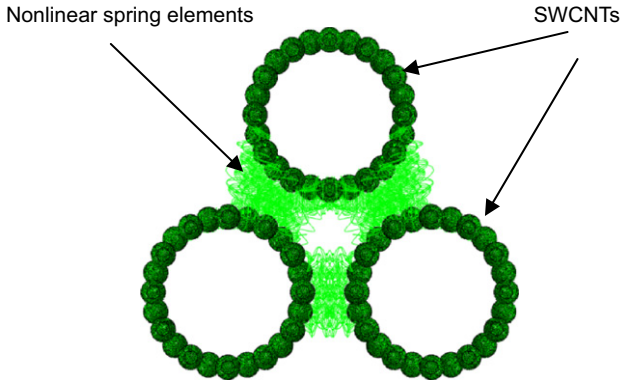

Fig. 3. Spring elements for simulating vdW interaction forces.

r corresponds to the distance between the interacting particles. A typical curve of the Lennard–Jones potential is given in Fig. 2.

In the structural system, the vdW forces due to noncovalent interactions are assumed to be resembled by nonlinear spring elements. The force acting in such a spring element can be obtained by differentiating Eq. (10) and is given by

$$F(r) = -\frac{dU(r)}{dr} = 24\frac{\varepsilon}{\sigma}\left[2\left(\frac{\sigma}{r}\right)^{13} - \left(\frac{\sigma}{r}\right)^{7}\right] \tag{11}$$

The vdW force acting along the connecting line between two interacting atoms is simulated by a nonlinear spring element. The compressive-force displacement relationship of these spring elements can be approximated through Eq. (11). It is assumed that displacement changes in inter-atomic distance are relative to the critical distance of 0.38 nm [14]. As shown in Fig. 2, when the inter-atomic distance is less than 0.8 nm, the Lennard–Jones force between atoms is not zero. All these atoms are found by using a MATLAB program, and then they are connected with nonlinear springs in the input file of ABAQUS. This structural model is developed for axial, torsional and bending buckling analysis of CNT bundles as it is illustrated in Fig. 3.

3. Results and discussion

The commercial finite element numerical package ABAQUS was applied to study the critical buckling load of fixed–fixed, simple–simple and fixed–free CNT bundles. In addition, CNT bundles were studied with various interval distances under torsional and bending buckling analysis with and without vdW interactions. The critical buckling loads and torques are predicted by the present structural model. Armchair (7, 7) SWNTs with various aspect ratios (L/D) were employed for this study. The effect of vdW forces on the critical buckling loads and torques was also studied for armchair CNT bundles with various aspect ratios.

3.1. Axial buckling of CNT bundle

The critical buckling loads as well as the influence of boundary conditions on these were predicted by the present structural model. Armchair (7,7) SWNTs with various aspect ratios were employed for this study. Here, we fix two planes at the ends of bundle and apply an unaxial force to the center of the two planes. Moreover, different boundary conditions were applied to the atoms at both ends of CNT bundle. Fig. 4 shows the critical axial buckling loads of CNT bundles with different aspect ratios for three boundary conditions without vdW interaction forces. The critical buckling loads are obtained by our present model, and are compared with results from Liew et al. [6]. There are limited resources that investigated the axial buckling of bundle nanotubes. From the plot, it can be seen that as the aspect ratio of the individual SWCNT in a CNT bundle increases, its critical buckling load decreases exponentially. Also, the critical buckling load of the CNT bundles of three tends to reach a minimum value despite further increase in the aspect ratio. For high aspect ratios, maximum and minimum values of the critical buckling load occur for fixed–fixed and fixed–free boundary conditions, respectively.

When buckling occurs, the CNT bundles will undergo structural deformation. Fig. 5 shows the mode shapes of the compression process of CNT bundles for various boundary conditions and the aspect ratio of 6.602.

To compare the average critical buckling load of each tube with that of a SWCNT, values are presented in Table 2 for the fixed–fixed boundary condition. From Table 2, it is also evident that the average critical buckling load of each SWCNT in a CNT bundle of three without vdW interactions is very close to that of a SWCNT. It can therefore be deduced that the critical buckling loads for CNT bundles are directly proportional to the average critical buckling load of each SWCNT in the CNT bundle. This information allows simple computation of CNT bundles of up to hundreds of SWCNTs. To understand how the intertube vdW interactions affect the compressive properties of CNT bundles, two sets of structural simulations were carried out: (1) with vdW interactions and (2) without vdW interactions. Only the intratube vdW interactions were omitted in the calculations.

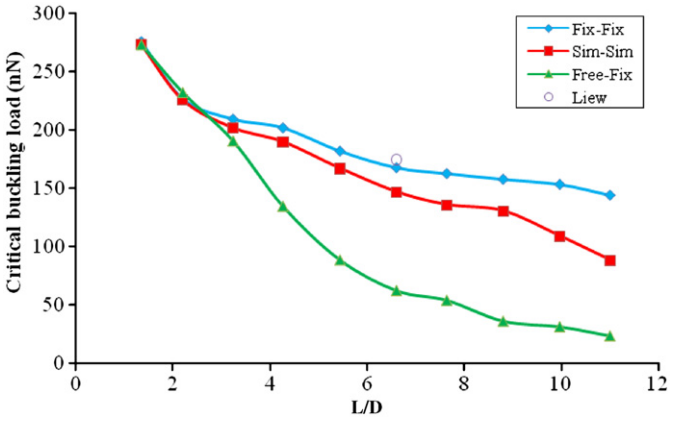

Fig. 4. Plot of critical buckling loads of CNT bundles of three as a function of the aspect ratio of SWCNT.

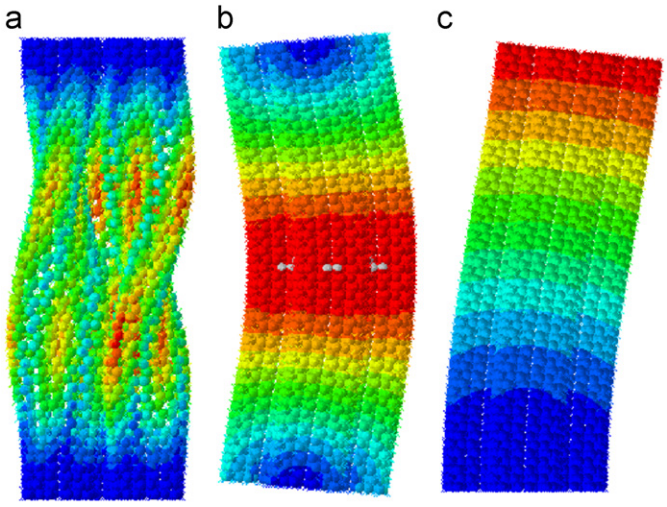

Fig. 5. The mode shapes of carbon nanotube bundle of (7,7) SWCNT under buckling analysis: (a) fixed–fixed, (b) simple–simple and (c) fixed–free.

Table 2
Comparison of average critical buckling load of CNT bundle of three with the buckling load of SWCNTs for the fixed–fixed boundary condition.

L/*D*	Average buckling load of bundle	Buckling load of SWCNT
1.3447	91.9933	93.1030
2.2	75.67	77.4630
3.236	69.823	72.4270
4.263	65.023	65.6910
5.437	60.67	59.1130
6.602	55.903	55.9020
7.6368	54.266	54.0500
8.800	52.603	52.4460
9.9670	51.13	51.4460
11.003	48.05	48.0640

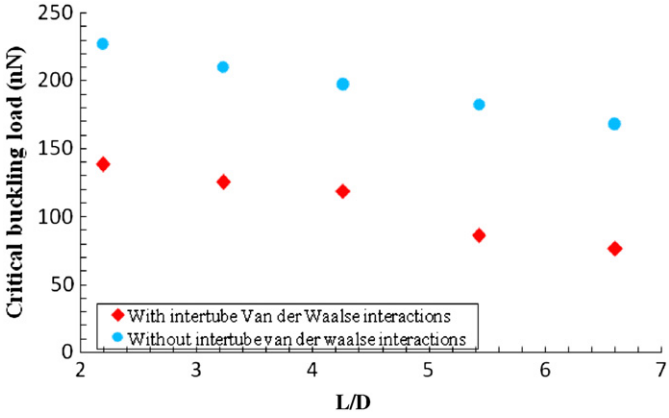

Fig. 6. Critical buckling loads of various aspect ratios of CNT bundles with and without intertube vdW interactions.

Fig. 6 shows the buckling loads for various aspect ratios of CNT bundles, with and without considering the intertube spring elements. From the figure, it is observed that despite having the same number of SWCNTs in the bundles, the critical buckling loads will decrease as the aspect ratio of the individual SWCNTs in the CNT bundles increases. However, the decreasing trends of the critical buckling loads are similar, it is revealed that higher buckling loads can be achieved when the intertube vdW interactions were not considered. This is in agreement with the findings of Liew et al. [10] and Lu [3] who reported that CNT bundles tend to have lower elastic moduli in comparison to individual SWCNTs due to the weak intertube vdW interactions that make the CNT bundles weaker, since the individual SWCNTs can easily rotate and slide with respect to one another.

3.2. Bending buckling of CNT bundle

In most models which have been presented in the mechanical behavior of SWCNT, one of the outputs which has been studied more is the critical buckling moment. In the modeling of structural models, various sizes of CNT bundles were used. These sizes are determined by the size of individual SWCNTs in the bundle. In this section, numerical results for armchair (7, 7) SWCNTs with different lengths are investigated. The effect of vdW forces on the critical bending buckling moment is also studied for the armchair CNT bundles with various aspect ratios.

As indicated in Fig. 7, two planes are attached to the ends of a CNT bundle and moments are applied to the center of the planes. Applied moments are in the direction of *X*-axis for the first plane and in opposite direction for the end plane. Figs. 8 and 9 show the critical buckling moment of CNT bundles with different aspect ratios with and without vdW interaction forces. Moments are applied in two directions of *X*-axis and *Y*-axis, as shown in Figs. 8 and 9, respectively.

Long tubes will behave like columns and buckle as a unit, while at shorter lengths will undergo shell wall buckling behavior. From the figures, it can be seen that the critical buckling moments of bundle nanotubes are higher than those of single nanotubes, and the critical moments of SWCNTs are approximately constant when shell mode shapes occur. Of course, it should be noted that for SWCNTs, the Euler mode will happen later at higher aspect ratios. The results also show that the bending buckling moments of bundle nanotubes with vdW interactions are lower than those of single nanotubes for aspect ratios greater than 5. This is because CNT bundles tend to have lower elastic moduli compared to individual SWCNT due to the weak intertube vdW interactions that make the CNT bundles weaker, as the individual SWCNTs can easily rotate and slide with respect to one another. The plot clearly demonstrates that for both the bundles, despite having the same number of SWCNTs when the vdW interactions are considered, the critical bending buckling moment decreases more rapidly as the aspect ratio increases. Therefore, vdW interaction forces have a great effect on the critical buckling moment of CNT bundle and dramatically, reduce the critical moment of bundles.

Apart from the above, structural simulations were performed at different interspatial gaps. This is to determine the size effect of the interspatial gaps on the buckling behaviors of CNT bundles. In this work, a total of three interspatial gaps were used, i.e. 0.22, 0.34 and 0.51 nm. Five different angles were also studied, i.e. 0°, 22.5°, 45°, 67.5°and 90°. Angle 0 is along the positive *X*-axis and values increase counter-clockwise from the positive *X*-axis in the *X*–*Y* plane as seen in Fig. 10. Fig. 11 shows the critical buckling moment applied to the center of two planes in various angles for the aspect ratio of 4.236. By increasing the angle between radius vector and *X*-axis, the critical buckling moment decreases and eventually reaches a constant value. By increasing the distance between the nanotubes the critical buckling moment increases. When the moment is applied about the *X* and *Y*-axis, the maximum and minimum moment is obtained, respectively. Minimum moment is related to the $\theta=90^{\circ}$, as this direction is coincident with the symmetry plane of bundle nanotube.

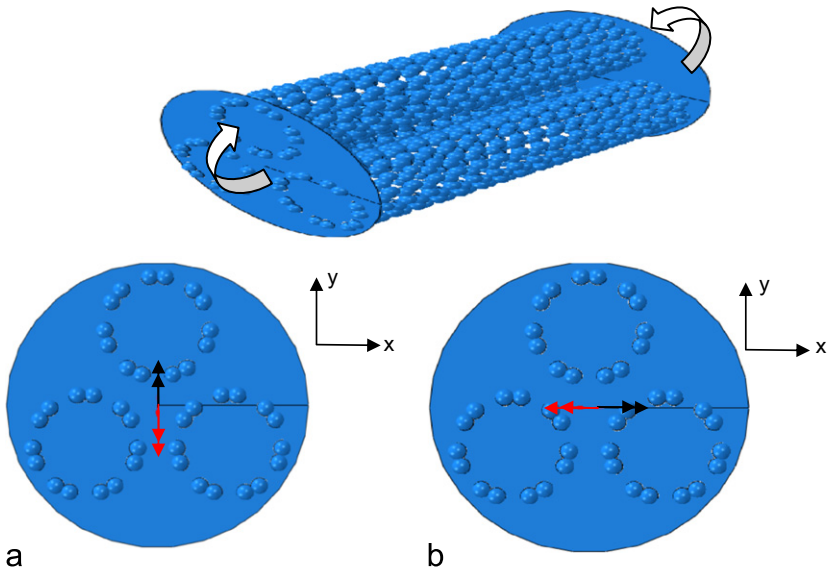

Fig. 7. Applied moments about (a) *X*-axis and (b) *Y*-axis.

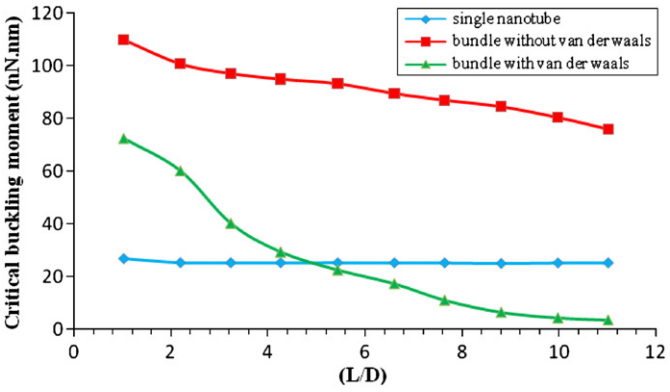

Fig. 8. Critical bending buckling moment of bundle nanotube with various aspect ratios, the moment is applied about *X*-axis.

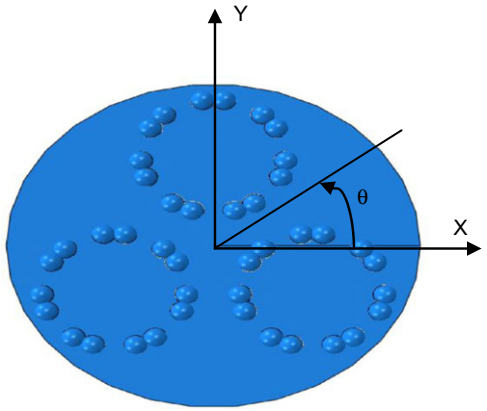

Fig. 10. θ variation in *X*–*Y* plane.

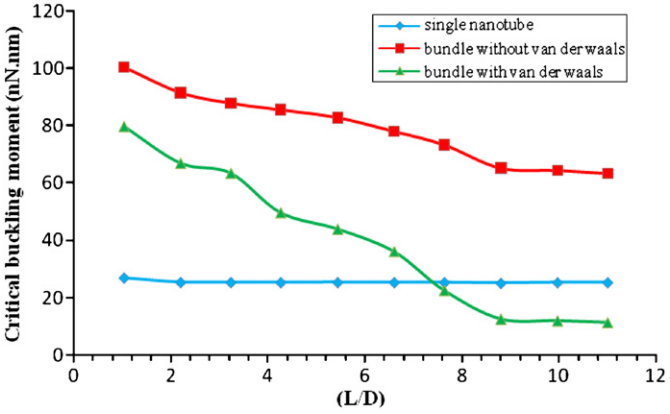

Fig. 9. Critical bending buckling moment of bundle nanotube with various aspect ratios, the moment is applied about *Y*-axis.

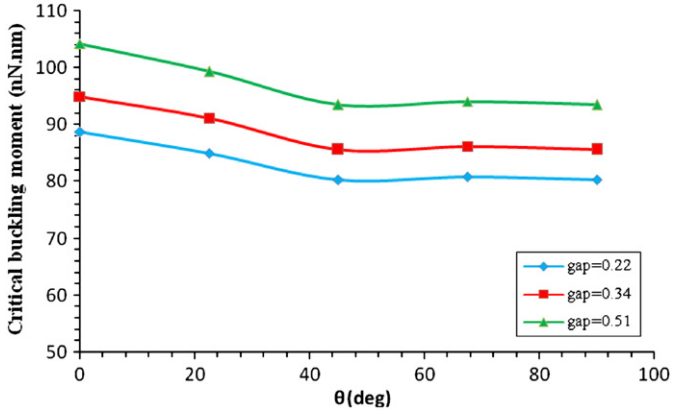

Fig. 11. Critical bending buckling moment of bundle nanotube with various angles for $L=4.058$.

Figs. 12 and 13 are shown to compare the critical buckling moment of CNT bundles versus the aspect ratio at various interval distances. Moments are applied about *X*-axis and *Y*-axis, as shown in Figs. 12 and 13, respectively. For different interval distances the moment about the *X*-axis leads to a greater value of critical buckling moment in comparison to the moment about the *Y*-axis. It is also seen that the bundle with the maximum interval gap has the maximum critical buckling moment for small lengths, but this

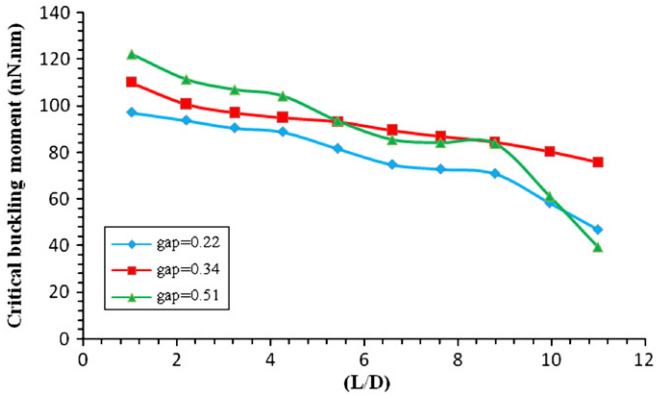

Fig. 12. Critical bending buckling moment of bundle nanotube with various aspect ratios, the moment is applied about *X*-axis.

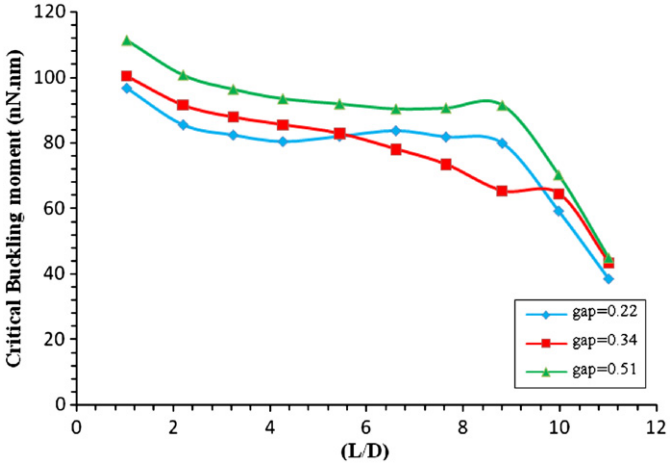

Fig. 13. Critical bending buckling moment of bundle nanotube with various aspect ratios, the moment is applied about Y-axis.

discipline is not seen for long lengths. This inconsistency occurs, due to their changes into the buckling mode shapes of CNT bundle. When bending buckling occurs, CNT bundles will undergo structural deformation. The mode shapes according to the displacement contours are represented for various bending buckling modes of perfect armchair bundles. Fig. 14 shows the mode shapes of the bundle of (7,7) SWCNT for the length of 6.272 nm under bending buckling moment. Moments are applied about *X*- and *Y*-axes. With the increasing aspect ratio, the shell mode shapes are converted to the Euler mode shape. As it can be seen all three tubes in bundle have not buckled at the same time which is in agreement with the results of Liew et al. [10].

3.3. Torsional buckling of CNT bundle

The critical buckling torque of CNT bundle has been predicted by the present structural model. Similar to the bending buckling analysis, two planes are attached to the ends of CNT bundle but a torque is applied to the center of one plane (see Fig. 15). It is seen from Fig. 16 that increasing the length of bundle nanotube decreases the critical buckling torque and also it is revealed that higher torsional buckling torque can be achieved when the intertube vdW interactions are considered. Apart from the above, it is observed that bundle SWCNT has more critical buckling torque than the single nanotube. In torsional buckling unlike bending buckling analysis, bundle with vdW interaction forces

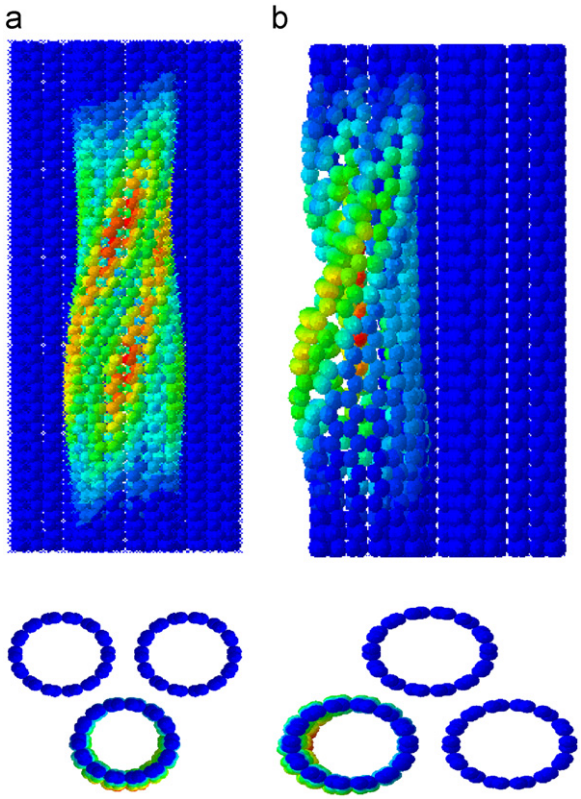

Fig.14. The mode shapes of bundle of (7,7) SWCNT $L=6.272$ nm, $D=0.95$ nm under bending buckling analysis: (a) moment in the direction of *X*-axis and (b) moment in the direction of *Y*-axis.

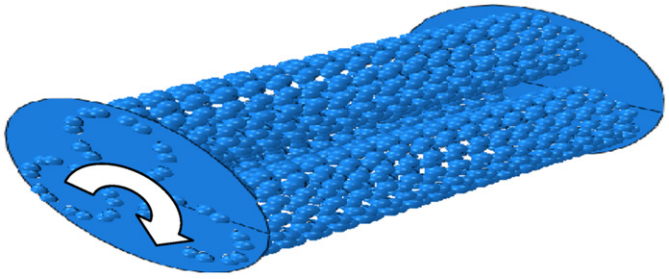

Fig. 15. Applied torque about *Z*-axis.

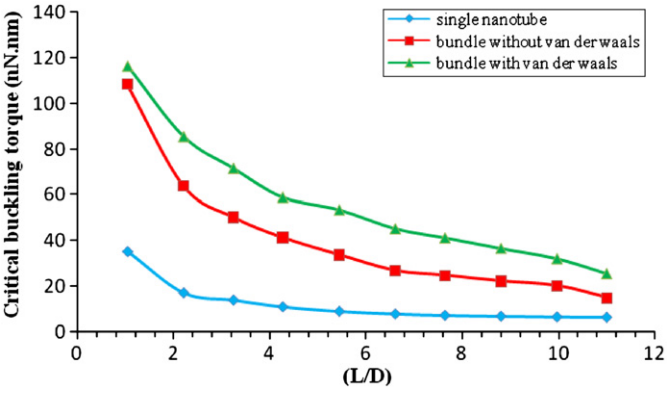

Fig. 16. Critical buckling torque of bundle nanotube with various aspect ratios, the torque is applied about *Z*-axis.

has a greater critical buckling torque than bundle without these interactions. Because in every mode shape of torsional buckling all the three SWCNTs are buckled simultaneously and they

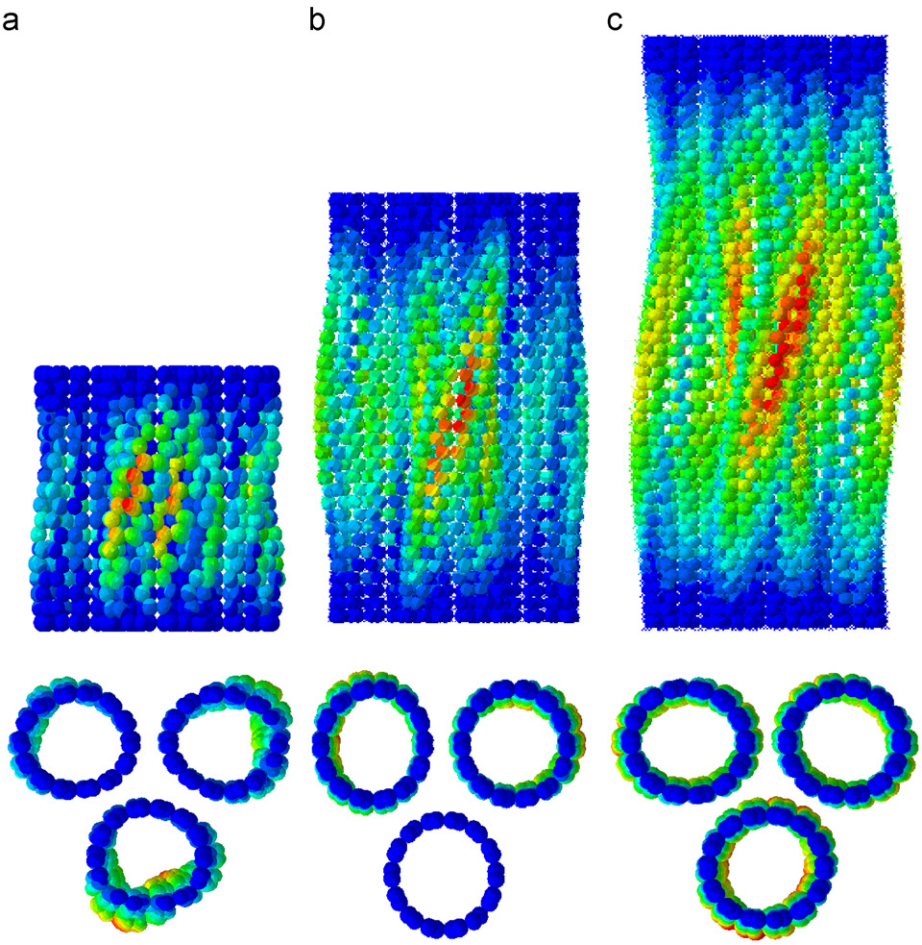

Fig. 17. The mode shapes of carbon nanotube bundle of (7, 7) SWCNT under torsional buckling analysis: (a) $L=2.09$ nm, (b) $L=4.058$ nm and (c) $L=6.272$ nm.

maintain their symmetry. The mode shapes according to displacement contours are represented for various lengths of bundle armchair nanotubes as in Fig. 17.

4. Conclusions

In the present paper, CNT bundles with fixed–fixed, simple–simple and fixed–free boundary conditions and various loadings were studied based on a structural mechanics approach using ABAQUS with and without intertube vdW interaction forces. In addition, CNT bundles were studied with various interval distances under bending and torsional buckling analysis with and without vdW interactions. Moreover, the critical torsional buckling for different sizes of CNT bundles at various interspatial gaps has been performed. From these investigations, the following results were obtained:

1. The intertube vdW interactions in a CNT bundle reduce the value of critical axial buckling loads.
2. By increasing the aspect ratio the critical buckling load will decrease and reaches a constant value.
3. The maximum and minimum critical buckling loads for an arbitrary aspect ratio occur at the fixed–fixed and fixed–free boundary conditions, respectively.
4. The rate of reduction of the critical buckling loads for the fixed–free boundary condition is higher than other boundary conditions.
5. The vdW interaction in a CNT bundle reduces the value of the critical bending buckling moment.
6. By increasing the aspect ratio the critical buckling torque will decrease.
7. The maximum and minimum critical buckling moments occur for a bundle with interval distances of 0.51 and 0.22 nm, respectively.
8. The degree that has maximum critical bending buckling moment, is $\theta=0^{\circ}$.
9. For small lengths, the CNT bundle with maximum interspatial gap has the maximum critical buckling moment but this discipline is not seen for long lengths.
10. In different interval distances, the moment, which is exerted about X-axis, has the maximum value of critical buckling moment.
11. In torsional buckling unlike bending buckling a CNT bundle with vdW interaction forces has a greater critical buckling torque than a CNT bundle without these forces.

References

[1] S. Ijima, Nature 354 (1991) 56–58.
[2] B.I. Yakobson, C.J. Brabec, J. Bernholc, Phys. Rev. Lett. 76 (1996) 2511–2514.
[3] J.P. Lu, Phys. Rev. Lett. 79 (1997) 1297–1300.
[4] J.P. Salvetat, G.A.D. Briggs, J.M. Bonard, R.R. Bacsa, A.J. Kulik, T. Stockli, et al., Phys. Rev. Lett. 82 (1999) 944–947.
[5] T. Chang, Appl. Phys. Lett. 90 (2007) 201910–201913.

[6] S.H. Yang, L.L. Feng, F. Feng, J. Phys. D: Appl. Phys 42 (2009) 055414.
[7] S.H. Yang, Z.X. Wei, Phys. Lett. A 373 (2009) 682–685.
[8] C.Q. Ru, Phys. Rev. B 62 (2000) 10405–10408.
[9] D. Qian, W.K. Liu, R.S. Ruoff, Compos. Sci. Technol. 63 (2003) 1561–1569.
[10] K.M. Liew, C.H. Wong, M.J. Tan, Acta Mater. 54 (2006) 225–231.
[11] B.I. Yakobson, L.S. Couchman, J. Nanopart. Res. 8 (2006) 105–110.
[12] S. Cranford, M.J. Buehler, Int. J. Mater. Struct. Int. 3 (2009) 161–178.
[13] V. Parvaneh, M. Shariati, A.M.Majd Sabeti, Eur. J. Mech. A—Solid 28 (2009) 1072–1078.
[14] W.D. Cornell, P. Cieplak, C.I. Bayly, et al., J. Am. Chem. Soc. 117 (1995) 5179–5197.
[15] V. Parvaneh, M. Shariati, Acta Mech. 216 (2011) 281–289.
[16] V. Parvaneh, M. Shariati, H. Torabi, Comp. Mater.Sci 50 (2011) 2051–2056.
[17] V. Parvaneh, M. Shariati, A.M. Majd Sabeti, H. Torabi, J. Nanomater. (2011) 297902.
[18] J.M. Haile, Molecular Dynamics Simulation: Elementary Methods, John Wiley and Sons, New York, 1992.
[19] J.H. Walther, R. Jaffe, T. Halicioglu, P. Koumoutsakos, J. Phys. Chem. B 105 (41) (2001) 9980–9987.